Acta Crystallographica Section B
Structural Science
ISSN 0108-7681

Non-covalent interactions in the crystallization of the enantiomers of 1,7-dioxaspiro[5.5]undecane (olive fly sex pheromone) by enantiospecific cyclodextrin hosts, hexakis(2,3,6-tri-*O*-methyl)-α-cyclodextrin and heptakis(2,3,6-tri-*O*-methyl)-β-cyclodextrin

Stella Makedonopoulou,[a] Konstantina Yannakopoulou,[a] Demetrios Mentzafos,[b] Victor Lamzin,[c] Alexander Popov[c] and Irene M. Mavridis[a]*

[a]Institute of Physical Chemistry, National Center for Scientific Research 'Demokritos', Aghia Paraskevi 153 10, Athens, Greece, [b]Physics Laboratory, Agricultural University of Athens, Iera Odos 75, 118 53 Athens, Greece, and [c]European Molecular Biology Laboratory, c/o DESY, Notkestrasse 85, D-22603 Hamburg, Germany

Correspondence e-mail: mavridi@mail.demokritos.gr

Received 24 November 2000
Accepted 30 January 2001

The enantiomers of racemic olive fly sex pheromone 1,7-dioxaspiro[5.5]undecane (1) have been isolated by crystallization with enantiospecific cyclodextrin hosts: (*S*)-(1) crystallizes with heptakis(2,3,6-tri-*O*-methyl)-β-cyclodextrin (TMβCD) and (*R*)-(1) with hexakis(2,3,6-tri-*O*-methyl)-α-cyclodextrin (TMαCD). The crystal structure of TMβCD/(*S*)-(1) from synchrotron radiation data at 100 K, determined for the first time, proves that TMβCD crystallizes with only the (*S*)-enantiomer from the racemic mixture. Comparison with the 100 K structure of TMαCD/(*R*)-(1) redetermined with synchrotron data has provided insight into the interactions between each of the hosts with the corresponding enantiomeric guests. Owing to the high resolution of the data and the unusually high quality of the crystals, localization of the H atoms has been achieved, a rare accomplishment for cyclodextrin X-ray structures. This made possible, apart from the geometry of the complexes, the detailed description of a five-membered-ring water cluster with very well ordered hydrogen bonding. The enantiospecificity exhibited by the described systems reveals the subtle differences of the weak intermolecular forces involved in the selective binding of the two optical antipodes by the two hosts. The binding geometry in the two complexes is different, but it is effected in both by numerous host–guest C—H$\cdots$O interactions, resulting from induced fit of the hosts toward each of the enantiomeric guests. In TMαCD/(*R*)-(1) two of these H$\cdots$O host–guest distances, directed toward the acetal O atoms defining the chirality of the guest, are much shorter than the rest and also shorter than all the H$\cdots$O distances in TMβCD/(*S*)-(1). Moreover, (*R*)-(1) interacts not only with the enclosing host, but with other hosts in the crystal lattice, in contrast to (*S*)-(1) in the TMβCD/(*S*)-(1) complex which is isolated inside channels formed by the host molecules. The above differences are reflected in the much higher binding constant of TMαCD/(*R*)-(1) compared with that of TMβCD/(*S*)-(1) ($\sim$6800 and $\sim$935 M^{-1}, respectively), determined by NMR in aqueous solution, and the ability of TMαCD to selectively precipitate (*R*)-(1) from racemic (1) in much higher yield than TMβCD precipitates (*S*)-(1).

1. Introduction

Chiral recognition, a process of prime importance in chemistry and biology, has been approached by studies with model molecular receptors able to bind selectively substrates by means of intermolecular interactions. High enantioselectivity is achieved by factors such as shape complementarity of

receptor–substrate and large area of contact (Lehn, 1995), requirements which are met in cyclodextrin host–guest systems. Cyclodextrins (CDs), cyclic oligosaccharides (I)

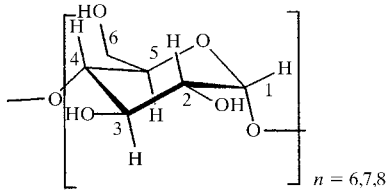

(I)

consisting mainly of six (αCD), seven (βCD) or eight (γCD) α-(1,4)-linked D-glucopyranosyl residues (Szejtli, 1998; Wenz, 1994) have a hydrophobic, relatively rigid cavity able to include a plethora of molecules. Therefore, the concept of maximum contact can be realised by the embracing of the guest by the host. In addition, by varying the number of glucose residues, stability and selectivity of the type 'lock and key' can be achieved for certain guest molecules which have the appropriate size and shape. In addition to the above 'lock and key' recognition, CDs in the form of their derivatives, can exhibit enhanced 'glove and hand' selectivity, resembling that of enzymes, by 'induced fit' binding of a guest. The term implies that the guest triggers conformational changes in the host in order to improve its complementarity towards the specific guest geometry.

It has been recognized early that CDs, as chiral hosts, form diastereomeric inclusion complexes with chiral substrates, a feature that provides CDs with the potential for enantiomeric discrimination, and this property is the basis of enantiomeric resolution by chiral gas and liquid chromatography (Schürig & Nowotny, 1990; Li & Purdy, 1992; König, 1991; Hilton & Armstrong, 1991; Köhler *et al.*, 1992). Enantiomeric discrimination by CDs is achieved by weak intermolecular interactions that may not include conventional hydrogen bonding. Therefore, chiral molecules lacking hydrogen-bond donor or acceptor groups have the potential to be resolved. Resolution of racemates by natural α-, β- and γCDs is very poor, with the partial resolution of fenoprofen [$(S)/(R)$ = 3/1] by βCD as the only exception (Hamilton & Chen, 1988). This is because the secondary hydroxyl groups (I) of adjacent glucose units form six, seven or eight strong intramolecular hydrogen bonds (Saenger, 1980) in α-, β- and γCD, respectively, of the type O2n—H$\cdots$O3(n + 1) that keep the cavity rigid and symmetrical (Saenger, 1980; Mentzafos *et al.*, 1991). As a consequence, strict shape complementarity with a particular chiral guest is required for complete enantioselective complexation. On the other hand, derivatization of cyclodextrins, especially per-derivatization at the secondary side, destroys the strong intramolecular hydrogen-bonding network and generates macrocycles which are more readily distorted from the geometry of the parent CDs (Harata *et al.*, 1984*a*) and, therefore, more suitable for enantiomeric discrimination *via* induced fit.

Indeed, X-ray studies (Harata *et al.*, 1984*a*, 1987, 1992; Caira *et al.*, 1996; Brown *et al.*, 1996; Caira *et al.*, 1995) have shown that the conformation of permethylated macrocycles can be remarkably distorted and the topology of the inclusion of optical antipodes is different (Harata *et al.*, 1984*b*, 1987, 1988). However, the ability of CDs as agents for selective precipitation of one enantiomer from solutions of racemic mixtures has been very limited (Harata *et al.*, 1988; Benshop & Van der Berg, 1970; Mokolajczyk & Drabowicz, 1971), except for the case of hexakis(2,3,6-tri-*O*-methyl)-α-cyclodextrin (permethylated αCD, TMαCD) and racemic 1,7-dioxaspiro-[5.5]undecane (1), where we have demonstrated that we can isolate exclusively the (*R*)-enantiomer (Yannakopoulou *et al.*, 1996). Spiroacetal 1 (II)

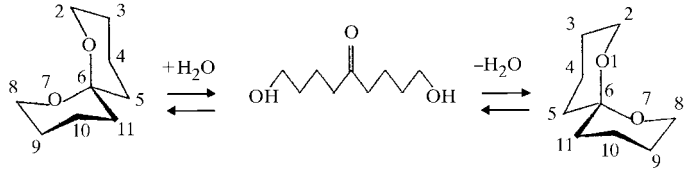

(*R*)-(−)-(1) (*R*)-(+)-(1)

(II)

is the major constituent of the sex pheromone of the olive pest *Bactrocera oleae* (Fletcher & Kitching, 1995) and is isolated from the insect as the racemic mixture. The pure antipodes, however, are of importance since (*R*)-(1) attracts the male and (*S*)-(1) the female insects (Mori, 1998). Therefore, the isolation of the enantiomers by simple precipitation/extraction methods is a really attractive alternative to tedious asymmetric syntheses. Presently, we have crystallized the inclusion complex of (*S*)-(1) with heptakis(2,3,6-tri-*O*-methyl)-β-cyclodextrin (TMβCD), a CD of different cavity size, again from aqueous solution. At this point, the determination of the highly accurate crystal structure of TMβCD/(*S*)-(1) and its comparison with that of TMαCD/(*R*)-(1), of higher accuracy, has provided insight into the interactions between each of the hosts with the corresponding enantiomeric guests. Owing to the high quality of the crystals, the data collection (synchrotron radiation) and the low temperature, localization of even the H atoms has been achieved, which is rare for cyclodextrin X-ray structures.

Binding studies in aqueous solution by NMR complement the studies in the crystalline state. The enantiospecificity exhibited by the systems described reveals the subtle differences of the weak intermolecular forces involved in the selective binding of the two optical antipodes by the two hosts. This kind of detailed analysis contributes to our understanding of the non-bonding interactions not only in the specific family of hosts but also of other complex systems such as proteins, which share the property of enantioselective binding (Breslow & Dong, 1998).

2. Experimental

2.1. General methods

NMR spectra were recorded on a Bruker AC 250 spectrometer. Optical rotation was measured on a Perkin-Elmer 241

Table 1
Experimental details.

	TMαCD/(*R*)-(1)	TMβCD/(*S*)-(1)
Chemical formula	$C_{54}H_{96}O_{30}\cdot C_9H_{16}O_6\cdot 5.1H_2O$	$C_{63}H_{112}O_{35}\cdot C_9H_{16}O_2\cdot 0.57H_2O$
Chemical formula weight	1471.24	1596.05
Cell setting, space group	Orthorhombic, $P2_12_12_1$	Orthorhombic, $P2_12_12_1$
a, b, c (Å)	14.636 (8), 21.637 (10), 23.45 (3)	10.936 (7), 25.53 (2), 29.64 (4)
V (Å^3)	7425 (11)	8275 (14)
Z	4	4
D_x (Mg m^{-3})	1.316	1.288
Wavelength (Å)	0.55000	0.65000
μ (mm^{-1})	0.066	0.103
Temperature (K)	100 (2)	100 (2)
Data collection		
No. of measured, independent and observed parameters	26 008, 26 008, 25 625	16 516, 16 516, 15 022
Criterion for observed reflections	$I > 2\sigma(I)$	$I > 2\sigma(I)$
R_{int}	0.0000	0.0000
θ_{max} (°)	30.61	30.00
Range of h, k, l	$0 \rightarrow h \rightarrow 27$ $0 \rightarrow k \rightarrow 39$ $0 \rightarrow l \rightarrow 43$	$0 \rightarrow h \rightarrow 16$ $0 \rightarrow k \rightarrow 39$ $0 \rightarrow l \rightarrow 45$
Refinement		
Refinement on	F^2	F^2
$R[F^2>2\sigma(F^2)]$, $wR(F^2)$, S	0.0289, 0.0823, 1.079	0.0624, 0.1831, 1.042
No. of reflections and parameters used in refinement	26 008, 1572	16 516, 1519
H-atom treatment	Mixed	Mixed
Weighting scheme	$w = 1/[\sigma^2(F_o^2) + (0.0465P)^2 + 0.3989P]$, where $P = (F_o^2 + 2F_c^2)/3$	$w = 1/[\sigma^2(F_o^2) + (0.1085P)^2 + 2.6761P]$, where $P = (F_o^2 + 2F_c^2)/3$
$(\Delta/\sigma)_{max}$	1.459	4.701
$\Delta\rho_{max}$, $\Delta\rho_{min}$ (e Å^{-3})	0.529, −0.423	0.682, −0.436

Computer programs used: *SHELXL*97 (Sheldrick, 1997).

polarimeter. Chiral gas chromatography was performed on a Varian 3300 instrument equipped with an Rt-βDex$_m$ column (30 m), Restek Corporation (70° isothermal run, injector temperature 493 K, detector temperature 373 K, He carrier gas, 11 p.s.i.).

2.2. Materials

TMαCD and TMβCD were commercial samples (Cyclolab) and used as received. 1,7-Dioxaspiro[5.5]undecane was purchased from Vioryl S.A., Athens, Greece. The solvents used were analytical grade and deuterated solvents were obtained from CORTEC, France.

2.3. Crystallization of TMαCD(*R*)-(1) inclusion complex

Colorless crystals of the complex were very readily grown from 10 m*M* aqueous solutions of synthetic racemic (1) and TMαCD, at room temperature. The exclusive isolation of (*R*)-(1) by its enantiospecific complexation with TMαCD has been fully documented by NMR, optical rotation measurements and chiral gas chromatography, as reported previously (Yannakopoulou *et al.*, 1996).

2.4. Crystallization of TMβCD/(*S*)-(1) inclusion complex

Colorless crystals of the complex were slowly grown inside NMR tubes, out of 0.5 ml aqueous solutions 63 m*M* in TMβCD and 34 m*M* in (±)-(1), at ambient temperature. The guest was obtained from the crystals after their dissolution in water and repeated extraction with pentane. The extract was examined by ^{13}C NMR in D_2O solution in the presence of a twofold excess of αCD, as the chiral shift reagent, by chiral gas chromatography based on a TMβCD column, and by polarimetry. Both NMR and GC methods agreed that the extract contained (*S*)-(+)-(1) (∼75%) and (*R*)-(−)-(1) (∼25%). A similar result was obtained from polarimetry ($[\alpha]_D$ = +80, pentane solution, c = 0.2), although the accuracy of this measurement was moderate.

2.5. Measurements of binding constants by NMR in aqueous solution

Solutions of TMβCD in D_2O (10 m*M*) were titrated at 298 K with either neat (*R*)-(1), obtained from the complex with TMαCD, or (*S*)-enriched-(1), and the displacement of the cavity proton H3 upon inclusion was monitored by ^{1}H NMR. (*S*)-Enriched-(1) was obtained from the solid complex with TMβCD. The complex precipitated (42%) from an aqueous solution of TMβCD (80 m*M*) and (±)-(1) (80 m*M*), after stirring for 24–48 h at ambient temperature. It was then completely dissolved in a water/pentane (8:1, v/v) mixture, and after repeated extraction with pentane the spiroacetal (51% from the complex) was recovered and identified as a mixture (*S*)-(1) (∼75%) and (*R*)-(1) (∼25%), by optical rotation, ^{13}C NMR in the presence of αCD as the chiral shift reagent and chiral chromatography, as described previously in the crystallization section.

The results of both titrations [chemical shift displacements of TMβCD cavity proton H3 *versus* the concentration of either (*R*)- or (*S*)-enriched-(1)] were analyzed with the non-linear regression routine provided by *GraphPad PRISM*.

2.6. X-ray crystallography

High-resolution X-ray data (Table 1) were collected using the synchrotron radiation light source of beamline BW7A at EMBL, DESY, Hamburg, by the oscillation method using a MAR image plate detector of 30 cm radius, unless otherwise stated. A single crystal, covered with a drop of oil, was mounted on a small loop of hair fiber and was instantly frozen at 100 K. Crystal data and experimental details of X-ray

analysis are given in Table 1. The programs *DENZO* and *SCALEPACK* (Otwinowski & Minor, 1997) were used for data processing and scaling of data, respectively. The unit-cell parameters were determined from the post refinement procedure, while their e.s.d.'s were from the unit-cell parameters of all the frames of data collected. Least-squares refinement on F^2 was carried out with the program *SHELXL*97 (Sheldrick, 1997).

2.6.1. TM*α*CD/(*R*)-(1) inclusion complex. The crystals were colorless prisms and of exceptional quality, unusual for a cyclodextrin inclusion complex, their diffraction extending beyond the 2θ range collected ($\sin\theta/\lambda = 0.94$ Å^{-1}, resolution 0.53 Å). Three separate sets of frames were collected, each by an overall rotation of the crystal by 90°:

(i) High-resolution data: 0.53 Å. 61 frames were obtained with a $\delta\varphi$ rotation of 1.5°, crystal-to-detector distance 80 mm and maximum $2\theta = 61.2°$.

(ii) Medium-resolution data: 0.72 Å. 44 frames were obtained with a $\delta\varphi$ rotation of 2.3°, crystal-to-detector distance 90 mm and maximum $2\theta = 45.0°$.

(iii) Low-resolution data: 1.72 Å using a MAR image plate detector of radius 18 cm. 30 frames were obtained with a $\delta\varphi$ rotation of 4.5°, crystal-to-detector distance 270 mm and maximum $2\theta = 18.4°$.

The three sets of images after indexing and processing were scaled and merged to a completeness of 99.2% with $R_{\rm merge}$ of 0.025.

The structure was solved by the Patterson vector search method with the program *PATSEE* (Egert & Sheldrick, 1985) using the glucosidic skeleton of the room-temperature data (Mentzafos *et al.*, 1999), crystallized in the space group $C222_1$. The rest of the cyclodextrin and water atoms were found by consecutive difference-Fourier calculations. After 12 cycles of full-matrix least-squares refinement, with data of low resolution, 0.8 Å, the R factor was 0.0703 for 8252 reflections with $F_o > 4\sigma(F_o)$. By then the atoms of the disordered guest were already located. The refined structure confirmed that the guest was the (*R*) enantiomer, with the O atoms in diaxial conformation: In the difference electron density map the one acetalic O atom was the most prominent peak, whereas the other, located at the exterior of the cavity, was of moderate peak height. By the end of the refinement, H atoms were revealed in all but two positions of the acetal rings, the latter being clearly the O atoms. Thus, it was proved that the absolute configuration assigned to the guest was correct. The refinement continued anisotropically for all the non-H atoms, with all the data (26 008/1572 reflections/final parameters), and converged to a final R_1 of 0.0289. The occupancy factors of the disordered guest molecules were refined to 45–55%. Almost all the H atoms of both host and guest were found by the difference Fourier method and were refined isotropically. The thermal parameters of both the host and guest atoms were very low and of the same order of magnitude, the highest of the guest being twice as large as the highest of the host. 5.1 water molecules, distributed over seven sites in the lattice were found, five of them with high occupancy for which H atoms were located, and two of very low occupancy.

2.6.2. TM*β*CD/(*S*)-(1) inclusion complex. Three separate sets of frames were collected:

(i) High-resolution data, 0.67 Å: 63 frames were obtained with 1.1° $\delta\varphi$ rotation, crystal-to-detector distance 85 mm and maximum $2\theta = 60.0°$.

(ii) High-resolution data, 0.67 Å: 40 frames were obtained with 2.5° $\delta\varphi$ rotation, crystal-to-detector distance 95 mm and maximum $2\theta = 57.6°$.

(iii) Low-resolution data, 1.79 Å: using a MAR image plate detector of radius 18 cm. 20 frames were obtained with 4.0° $\delta\varphi$ rotation, crystal-to-detector distance 235 mm and maximum $2\theta = 21.0°$.

The three sets of images after indexing and processing as before were scaled and merged to a completeness of 97.0% with $R_{\rm merge}$ of 0.037.

The structure was solved by a Patterson vector search and Fourier recycling method with *DIRDIF*94 (Beurskens *et al.*, 1994). Suitable models for searching the Patterson space were obtained from the TM*β*CD/ethyl laurate structure (Mentzafos *et al.*, 1994). Of the seven different models generated, each consisting of three sequential glucosidic residues, one gave the correct structure with all TM*β*CD and guest atoms, the latter disordered in two positions. After 18 cycles of full-matrix least-squares refinement, with data of 0.7 Å resolution, the R factor was 0.0821 for 12 710 reflections with $F_o > 4\sigma F_o$. The refinement continued anisotropically, for all the non-H atoms, with all the data (16 516/1549 reflections/final parameters).

The results of the characterization of the guest by means other than X-ray diffraction showed that the (*S*)-(1) coexisted with (*R*)-(1) (∼25%) and the open form of the guest, a fact indicating that racemization had occurred. Therefore, it was necessary to determine unambiguously whether in the crystalline state the guest was pure (*S*)-(1) or a mixture of the two enantiomers. The electron density corresponding to the guest was very well defined and the model of (*S*)-(1) with its tetrahydropyranyl rings in the chair conformation and the O atoms occupying diaxial positions fitted perfectly. The (*S*)-(1) geometry was exactly the same as that of (*S*)-(1) in the inclusion complex (2a,2b,2c,2d,2e,2f,3a,3g,6a,6b,6c,6d,6e,6f,6g-pentadeca-*O*-methyl)-*β*CD/(*S*)-(1) (Rysanek *et al.*, 1992). As in the case of TM*α*CD/(*R*)-(1), only one O atom had the highest electron density in the difference electron density map. If (*R*)-(1) coexisted in the crystal, it should fit into the guest's density and its conformation should have been such that one of its rings should coincide with that of the (*S*)-(1), while in the other ring O7 should interchange with C11 (II). This would correspond to an energetically unfavorable conformation of (*R*)-(1) with the O atoms in the axial–equatorial positions. Along the refinement process, when H atoms were revealed, next to the spiro-carbon atom on both acetalic rings only two atoms were not bonded to any H atoms. The other two were found bonded to one or two H-atom(s), indicating that those were the C atoms. Thus, the location of

[1] Supplementary data for this paper are available from the IUCr electronic archives (Reference: NS0005). Services for accessing these data are described at the back of the journal.

Table 2
Conformations of the macrocycles.

d_1: deviations from the optimum plane of the six O4n atoms (with e.s.d.s in parentheses); d_2: O4$n\cdots$O4($n+1$) distances; φ: O4($n-1$)$\cdots$O4$n\cdots$O4($n+1$) angles; α: tile angles between the optimum O4n plane and the mean plances through atoms O4($n-1$), C1n, C4n and O4n (with e.s.d.s in parentheses); d_{6-5}: H6n—O5($n+1$) distances (Å) and angles (°) of C6n—H6$n\cdots$O5($n+1$); D_{2-3}: O3$n\cdots$O2($n+1$) distances.

	d_1 (Å)	d_2 (Å)	φ (°)	α (°)	d_{6-5} (Å)	D_{2-3} (Å)	Torsion angles C4n—C5n—C6n—O6n (°)	Torsion angles C5n—C6n—O6n—C9n (°)	Torsion angles C1n—C2n—O2n—C7n (C3n—C2n—O2n—C7n) (°)	Torsion angles C2n—C3n—O3n—C8n (C4n—C3n—O3n—C8n) (°)
TMαCD/(*R*)-(1)										
G1	−0.426(1)	4.25	115.2	35.99 (7)	2.54 (148.7)	3.36	−177.84(5)	71.2 (1)	61.09 (7) [−177.05 (5)]	−106.03 (7) [130.40 (8)]
G2	0.313 (1)	4.37	126.9	26.47 (7)	2.69 (141.4)	3.33	−173.06 (5)	−173.57 (7)	75.42 (7) [−164.50 (5)]	−100.91 (6) [138.02 (6)]
G3	0.133 (0)	4.35	114.3	9.16 (7)	2.36 (139.2)	3.89	44.42 (7)	81.58 (9)	103.97 (8) [−131.47 (8)]	−148.48 (6) [90.11 (7)]
G4	−0.460 (1)	4.22	114.5	39.38 (8)	2.51 (151.4)	3.41	−169.97 (6) 167.1 (7)	−174.10 (7) 84 (2)	58.61 (7) [−179.52 (5)]	−103.49 (7) [133.37 (8)]
G5	0.337 (5)	4.33	128.0	27.68 (7)	2.57 (146.3)	3.47	174.11 (5)	170.97 (6)	74.03 (8) [164.60 (6)]	108.37 (6) [130.35 (6)]
G6	0.102 (3)	4.24	115.1	7.47 (7)	2.38 (139.0)	3.74	43.19 (7)	85.42 (8)	117.90 (7) [−117.78 (7)]	−138.02 (6) [98.83−(6)]
TMβCD/(*S*)-(1)										
G1	−0.547 (2)	4.46	116.7	27.3 (2)	2.36 (144.8)	3.81	43.8 (4)	158.4 (3)	71.9 (3) [−165.4 (3)] 135.5 (17) [−98 (2)]	−134.7 (3) [102.1 (3)]
G2	0.361 (2)	4.56	144.6	56.9 (1)	–	4.11	−173.8 (4) 59 (1)	179.6 (6) 179 (3)	61.6 (3) [−173.4 (2)]	−98.1 (4) [138.5 (3)]
G3	0.350 (2)	4.26	124.3	7.7 (2)	2.37 (136.1)	3.50	48.0 (3)	82.7 (3)	142.1 (4) [−92.0 (4)]	−133.4 (3) [107.1 (3)]
G4	−0.491 (2)	4.30	114.8	27.33 (9)	2.26 (139.0)	3.49	−170.6 (2)	170.9 (3)	56.6 (2) [179.5 (2)]	−111.5 (3) [125.2 (3)]
G5	−0.090 (1)	4.61	137.9	41.0 (1)	2.73 (150.0)	3.26	−163.0 (2)	179.2 (3)	64.6 (3) [−173.3 (2)]	−94.7 (3) [144.3 (2)]
G6	0.423 (2)	4.44	132.0	6.4 (1)	2.57 (120.8)	3.25	48.7 (3)	−175.1 (2)	125.0 (2) [−109.4 (3)]	−122.5 (2) [118.7 (3)]
G7	−0.006 (2)	4.32	121.9	13.7 (2)	2.47 (129.8)	3.40	52.0 (3)	178.8 (3)	71.1 (3) [−164.6 (3)]	−103.8 (3) [136.4 (3)] −95 (4) [121 (4)]

the O atoms and consequently the absolute configuration of the guest were proven unequivocally and this is (*S*)-(1). The anisotropic refinement continued and converged to a final R_1 = 0.0619. The occupancy factors of the disordered guest molecule were refined to 48–52%. The host's and most of the guest's H atoms, found by the difference Fourier method, were assigned temperature factors 125% of the corresponding C atom. Although many factors, such as the shape of the electron density of the guest, the appearance of the H atoms in positions 5 and 11 of the guest's model and the smooth completion of the refinement resulting in low thermal parameters of the guest, convinced us that the guest was the (*S*) enantiomer, we nevertheless attempted an independent refinement with a mixture of (*S*)-(1) and (*R*)-(1) (in the axial–equatorial conformation) as the guest. However, it resulted in a distorted geometry of the molecules and worse statistics than the previous refinement and it was finally abandoned. During the later stages of the refinement two water positions of low occupancy were located. The maximum residual density of 0.68 e Å^{-3} is exaggerated, because it is located very close to the pseudotwofold axis.

3. Results and discussion

3.1. Binding of (*S*)-(1) with TMβCD and the high-resolution structure of the complex

The structure determination was based on high-resolution X-ray data (0.67 Å) and, as was shown in the *Experimental*, the absolute configuration of the guest was established. The asymmetric unit consists of one molecule of the complex TMβCD/(*S*)-(1) with the guest disordered over two positions (occupancies 52 and 48%). The TMβCD/(*S*)-(1) building blocks align head-to-tail in channels along the **a** crystallographic axis, the orientation of the supermolecules in neighboring channels being opposite (Fig. 1). This packing is observed for the first time in TMβCD structures. The guest is completely isolated within the channels.

One of the methoxy groups of the primary side is disordered: major conformation, O62—C92*a*, with occupancy

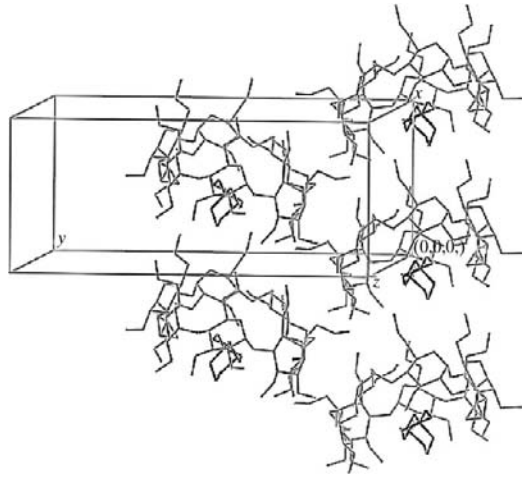

Figure 1
Packing of TMβCD/(*S*)-(1) inclusion complex.

70.4%; minor conformation, O62—C92*b* (Fig. 2). All glucose moieties have the $^4C_1$ chair conformation. There is extensive distortion of the macrocycle, as reflected in the geometrical parameters of the heptagonal ring formed by the glucosidic O4*n* atoms (Table 2). The heptagon's distances and angles, the distances of the O4*n* atoms from their mean plane and the tilt angles, that show the degree of tilting of the glucose residues with respect to the above mean plane, all vary widely among the residues and deviate from the corresponding parameters of the complexes of β-cyclodextrin, which exhibits sevenfold symmetry. The tilting is towards the interior of the cavity, as in the inclusion complexes of TMβCD/ethyl laureate (Mentzafos *et al.*, 1994) and TMβCD/methylcyclohexane (Rontoyianni *et al.*, 1998) and in contrast to all the other TMβCD complexes determined so far, where two glucose units tilt in the opposite sense (Harata *et al.*, 1992; Caira *et al.*, 1996; Brown *et al.*, 1996; Caira *et al.*, 1995; Harata *et al.*, 1983, 1988). Table 2 refers also to the conformation of the methoxy groups. Of the primary methoxy groups, three C6*n*—O6*n* bonds of residues G2 (major conformation), G4 and G5 point inward, making several CH···O close contacts (Fig. 2). The net result of this conformation, in combination with the strong tilting of residues G2 and G5, is that the primary side of the cavity over the guest (residues G1–G5) is sealed, whereas above residues G6 and G7 the primary side is open, as the methoxy groups of the latter residues point outward and do not participate in hydrogen bonding.

Disorder is also observed at the secondary methoxy groups MeO2 (occupancy of major component 86.9%) and MeO3 (occupancy of major component 83.9%) of residues G1 and G7, respectively. The major components of the above groups and the rest of the methoxy groups of the secondary side exhibit the usual conformation of the TMβCD complexes, but with a high degree of variation in their torsion angles (Table 2). We believe that this variation is due to the interactions of the atoms at the secondary side of the macrocycle with the guest (*see below*). Two water molecules of low occupancy are observed in the interchannel space, close to the two disordered methoxy groups of the secondary side. Some close contacts of one water molecule with H atoms of these methoxy groups are rather short and, since the occupancies of the water molecules are approximately supplementary to them, one may assume that the water molecules take their place when they move to their alternative positions. If we exclude the above interactions, the coordination of the waters is distorted tetrahedral involving two O—H···O and two C—H···O close contacts.

The (*S*)-(1) enantiomer, disordered over two positions related by a non-crystallographic pseudo-twofold axis, is situated off-center in the secondary side of the TMβCD macrocycle, whereas the cavity at the primary side is sealed above the guest, as mentioned previously. Its tetrahydropyranyl rings are in a chair conformation. Atoms O1, C2, C4 and C5 and O7, C8, C10 and C11 of both disordered sites of (*S*)-(1) lie in perfect planes forming mutual angles of 53.4 and 58.3°. Fig. 3 shows two views of TMβCD/(*S*)-(1). In Fig. 3(*a*) it is shown that, as the host's glucose residues G3 and G6 are almost parallel, the cavity flattens. In contrast, 90° around the macrocycle's axis the host–guest view is completely different (Fig. 3*b*). The cavity widens as residues G2 and G5 and, to a lesser extent, G1 and G4, tilt inward and approach each other at the primary side, while open up at the secondary side. The above interactions are better visualized in Fig. 4 (depicted as in Fig. 3) that plots the difference electron density corresponding to (*S*)-(1) and the van der Waals surface computed for TMβCD. Fig. 4(*a*) shows that the macrocycle forms a groove along (*S*)-(1), where the latter fits exactly. In Fig. 4(*b*) it is seen that the cavity becomes wide, harmonizing with the

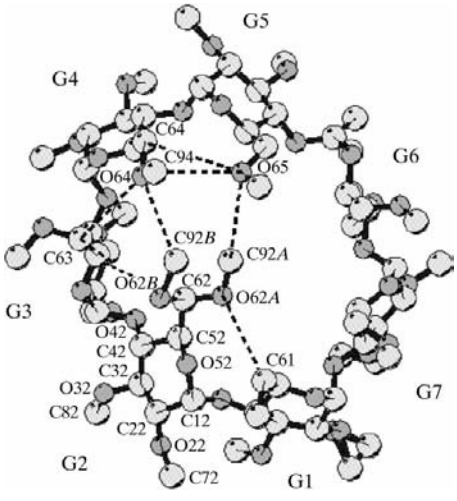

Figure 2
TMβCD conformation and numbering scheme: C*mn* or O*mn* denote the *m*th atom within the *n*th glucosidic residue (G*n*). Dotted lines indicate C—H···O close contacts in the macrocycle.

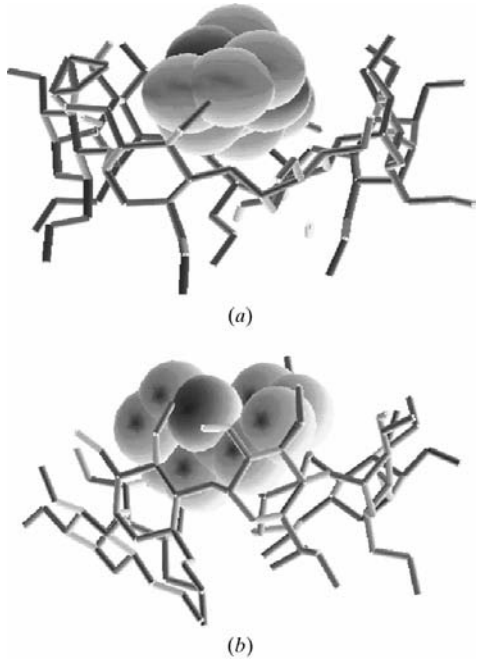

Figure 3
Two views of the TMβCD/(*S*)-(1) inclusion related by a 90° rotation about the molecular axis.

guest's length, but the fitting of the host with the ends of the guest is very loose.

As seen in Table 3, the intermolecular H···O distances (< 3.0 Å) between host and guest are numerous and of the type C—H···O and exhibit a high degree of directionality, *i.e.* C—H···O angles do not deviate much from linearity (Steiner & Desiraju, 1998; Steiner, 1997). Two important features are observed:

(i) the host–guest contacts are exclusively with the enclosing host and not with the lattice and, most importantly,

(ii) all contacts are quite long.

The range of distances varies between 2.54 and 2.98 Å, with the majority above 2.70 Å. However, the magnitude of the thermal parameters of the guest are of the same order compared with those of the host (some of them being at the most twice as large), in contrast to other CD complexes.

The (*S*)-spiroacetal extracted either from grown crystals or from bulk preparation of the complex was always contaminated with 25% of the (*R*)-enantiomer, even after very careful handling. This is explained by the systematic observation of the open ketodiol form of (1) [see (II)] in the extract, evidenced by a triplet at 2.54 p.p.m. in the ^{1}H and four extra peaks in the ^{13}C NMR spectra in D_2O, all at frequencies higher than those of (1). The identity of the open form was further verified by addition of TMβCD in a dilute aqueous solution of racemic (1), whereupon the four normal spiroacetal ^{13}C signals doubled due to the *in situ* formation of diastereoisomers TMβCD/(*S*)-(1) and TMβCD/(*R*)-(1), whereas the four extra signals, attributed to the achiral open form, were not affected. The association constant of TMβCD/(*S*)-enriched-(1) is 953 ± 93 M^{-1} (R^2 = 0.9989), moderate in absolute value but approximately three times larger than that of TMβCD/(*R*)-(1), which is K = 370 ± 33 M^{-1} (R^2 = 0.9988). These values show that the enantioselectivity of TMβCD toward the (*S*)-(1) is high and if this enantiomer did not partially revert to the (*R*)-(1), during its isolation, the binding constant would be even higher. The higher flexibility of the TMβCD macrocycle may be responsible for the fact that the binding constants are smaller in these complexes compared with those of TMαCD (see below) and does not result in high yield separation of the (*S*)-(1) from the racemic mixture.

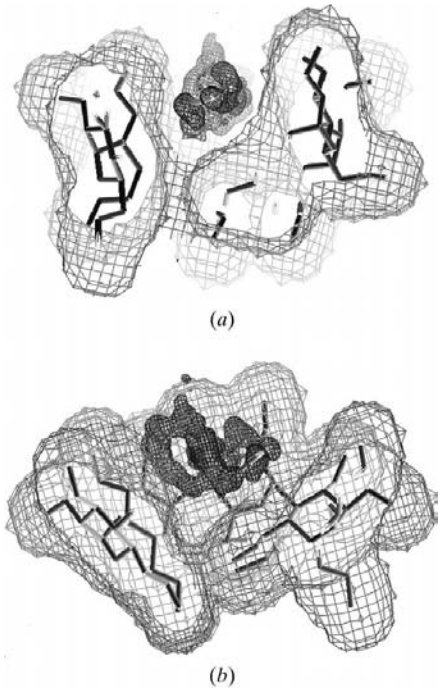

Figure 4
TMβCD/(*S*)-(1) inclusion complex. Calculated van der Waals surface of the host (the front has been removed for clarity reasons) and experimental difference electron density corresponding to the guest molecules, depicted as in Fig. 3.

Table 3
Close host–guest contacts.

Host	Guest	C···O (Å)	H···O (Å)	C—H···O (°)
TMαCD/(*R*)-(1)				
C86—H86$_3$	O1*A*	3.36	2.38	174
C33—H33	O7*A*	3.68	2.80	151
C83—H83$_2$	O7*A*	3.32	2.39	163
O26	H2$_1$*A*—C2*A*	3.58	2.89	126
O31^{i}	H4$_2$*A*—C4*A*	3.78	2.89	152
O23	H5$_2$*A*—C5*A*	3.58	2.60	142
O44	H8$_2$*A*—C8*A*	3.72	2.82	148
O41	H10$_1$*A*—C10*A*	3.57	2.66	167
O42	H11$_2$*A*—C11*A*	3.54	2.74	156
C33—H33	O1*B*	3.67	2.91	137
C83—H83$_2$	O1*B*	3.20	2.28	160
C84—H84$_2^{ii}$	O7*B*	3.79	2.94	137
C86—H86$_3$	O7*B*	3.38	2.48	153
O23	H2$_2$*B*— C2*B*	3.32	2.75	115
O41	H8$_1$*B*—C8*B*	3.81	2.95	146
O44	H10$_1$*B*—C10*B*	3.67	2.87	138
O26	H11$_2$*B*—C11*B*	3.81	2.96	150
O45	H11$_2$*B*—C11*B*	3.55	2.73	147
TMβCD/(*S*)-(1)				
C86—H86*C*	O1*A*	3.45	2.86	111
O26	H*A*3†—C3*A*	3.82	2.86	164
O45	H*A*3$_2$†—C3*A*	3.78	2.98	139
O44	H*A*4$_1$†—C4*A*	3.56	2.62	173
O45	H*A*5$_2$—C5*A*	3.57	2.75	130
C33—H33	O7*A*	3.75	2.77	166
O23	H*A*8$_1$—C8*A*	3.67	2.82	140
O47	H*A*10$_2$—C10*A*	3.60	2.54	166
O62	H*A*11$_1$†—C11*A*	3.68	2.69	173
O46	H*A*11$_2$—C11*A*	3.62	2.87	175
C33—H33	O1*B*	3.72	2.80	154
C83—H83*C*	O1*B*	3.50	2.68	134
O44	H*B*2$_1$†—C2*B*	3.60	2.80	134
O45	H*B*2$_2$—C2*B*	3.73	2.86	147
O26	H*B*4$_2$—C4*B*	3.66	2.76	148
C36—H36	O7*B*	3.59	2.77	157
C86—H86*C*	O7*B*	3.52	2.79	120
O46	H*B*8$_1$—C8*B*	3.62	2.58	172
O62	H*B*8$_2$—C8*B*	3.69	2.81	136
O42	H*B*10$_1$—C10*B*	3.63	2.74	157

Symmetry codes: (i) $-1-x,\frac{1}{2}+y,\frac{3}{2}-z$; (ii) $-1-x,-\frac{1}{2}+y,\frac{3}{2}-z$. † Calculated H atoms.

3.2. Binding of (*R*)-(1) with TMαCD and the high-resolution structure of the complex

The accurate data collected at 100 K and the exceptional quality of the crystals of this complex enabled us to determine the fine details of the structure not accessible in the room-temperature (RT) structure determined previously (Ment-

zafos *et al.*, 1999). The overall geometry of the complex and the topology of the binding, observed at low temperature (LT) is the same as in the RT structure. The space group of the latter had higher symmetry, where both the host and guest molecules were related by an exact crystallographic axis, whereas in the present, LT structure by a local non-crystallographic axis, the phase transition having occurred by the cooling of the crystals. The arrangement of the supermolecules in the crystal lattice (Fig. 5) differs from all known TMαCD structures. The TMαCD/(*R*)-(1) building blocks lay in unevenly spaced layers arranged in a head-to-tail fashion along the **c** crystallographic axis.

As opposed to the three water molecules of the RT structure, here there are five water molecules of 100% occupancy in the lattice, one of which is disordered over two positions (the high occupancy W35, 89% and the low W2, 12%), plus an additional water molecule, W1, of very low occupancy (12%) (Fig. 6). All are located between TMαCD layers separated by a wide space where part of the guest is also accommodated (Fig. 5). H atoms have been identified for all water molecules, except for those of low occupancy, therefore, it has been possible to characterize their association pattern. The high-occupancy water molecules form a cluster in the form of a pentagon, the apices of which are occupied by water O atoms, each donating one H atom to a neighboring water and another to a TMαCD O atom outside the pentagon and accepting a H atom from the other neighboring water. The hydrogen bonding in the pentagon is homodromic (Zabel *et al.*, 1986). The overall coordination of each water molecule is distorted planar trigonal. However, close contacts are observed between water molecules and H atoms bonded to C atoms of the macrocycle, each water oxygen forming one, and sometimes two, additional C—H$\cdots$O hydrogen bonds. It is worth noticing that a five-membered ring water cluster has been observed in the cavity of βCD in a neutron diffraction study at 120 K (Zabel *et al.*, 1986). Since the environment of the βCD cavity, lined by ether O atoms, resembles that of the periphery of permethylated CDs, it is possible that water clustering is favored in an environment lacking proton donors but rich in proton acceptors.

The TMαCD glucose moieties Gn have the $^4C_1$ chair conformation (Fig. 7). The primary methoxy group of residue G4 shows a disorder between a major conformation (O64a—C94a, occupancy = 92.2%), pointing outward, and a minor one (O64b—C94b, occupancy = 7.8%), pointing inward. Although the geometry of the hexagon formed by the glucosidic O4*n* atoms (Table 2) does not deviate much from that of a regular hexagon, the macrocycle is not symmetrical around the molecular axis, as observed in the inclusion complexes of αCD. The degree of deviation from the hexagonal symmetry is reflected mainly in two parameters, as shown in Table 2:

(i) the distance of the glucosidic O4*n* atoms from their optimum mean plane, ranging between −0.46 and 0.34 Å, is the highest observed in the TMαCD inclusion complexes determined so far (Harata *et al.*, 1987; Harata, 1990; Harata,

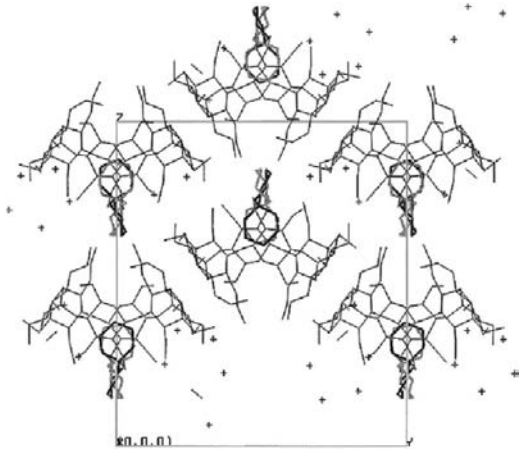

Figure 5
Packing of TMαCD/(*R*)-(1) inclusion complex.

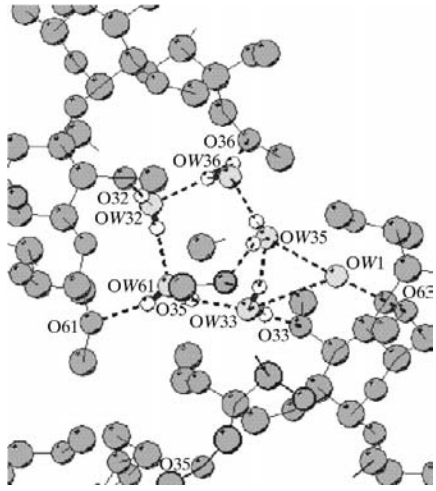

Figure 6
TMαCD/(*R*)-(1) inclusion complex. Geometry of the water cluster.

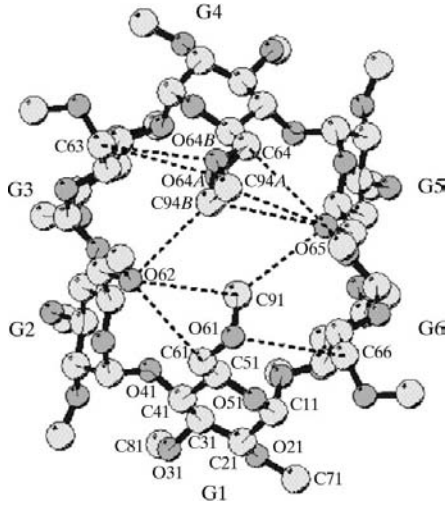

Figure 7
TMαCD conformation and numbering scheme: C*mn* or O*mn* denote the *m*th atom within the *n*th glucosidic residue (G*n*). Dotted lines indicate C—H$\cdots$O close contacts in the macrocycle.

Uekama, Otagiri & Hirayama, 1982*a*,*b*; Harata, Uekama, Otagiri, Hirayama & Sugiyama, 1982) and comparable to those of anhydrous TMαCD (Steiner & Saenger, 1996).

(ii) the tilting inwards of residues G1, G2, G4, G5 (range of the tilt angles 7.47–39.38°) which presents more variation in this complex compared with the other complexes of TMαCD. It is apparent from Table 2 that the two halves of the macrocycle are related by a pseudotwofold axis, the same one relating the two positions of the guest.

Table 2 also describes the geometry of the methoxy groups. In the primary side, four C6*n*—O6*n* bonds, in residues G1, G2, G4 and G5 that have high tilt angles, point inward and establish several C—H···O contacts among themselves (Fig. 7). Of the O6*n*—C9*n* bonds, only two, O6—C9 of G1 and O6—C9*b* of G4, point inward. The other four, as well as all methoxy groups of the least tilting residues G3 and G6, point outward, apparently for steric reasons. The overall effect of the excessive tilting of the four glucose residues is that they close the cavity at the primary side, while they widen it at the secondary side. At the same time, the small tilting of residues G3 and G6 flattens the cavity and brings the methoxy groups of C3 closer to the guest (Fig. 8*a*). This geometry matches the shape of the guest molecule as it is discussed next. The methoxy groups at the macrocycle's secondary side have the orientation common to TMαCD inclusion complexes, *i.e.* the O2*n*—C7*n* bonds point toward the exterior of the cavity, while O3*n*—C8*n* point toward the interior. It is remarkable that the bonds O33—C83 and O36—C86, whose atoms form very close contacts with the guest, have different conformations than the remaining O3*n*—C8*n* bonds (*see below*).

(*R*)-(1) is partially enclosed in the secondary side of TMαCD (Fig. 8). Its tetrahydropyranyl rings are in the chair conformation with the O atoms occupying diaxial positions, as expected. Atoms O1, C2, C4 and C5 and O7, C8, C10 and C11 of both disordered sites of (*R*)-(1), lie in perfect planes forming almost equal mutual angles of 53.4 and 54.1°, almost the same as in TMβCD/(*S*)-(1). The difference electron density, corresponding to (*R*)-(1), complements the van der Waals surface computed for the host macrocycle (Fig. 9) and suggests close contacts. Indeed, Table 3 lists numerous intermolecular contacts between host and guest of the type C—H···O with distances H···O < 3.0 Å. These are observed mainly between the guest and the enclosing host but, in contrast to TMβCD/(*S*)-(1), with adjacent hosts in the lattice also. The latter might explain the easy crystallization of the complex in high yields. The directionality of the interactions is high, since most of the C—H···O angles do not deviate much from linearity even for H···O distances longer than 2.7 Å, in contrast to analogous interactions in similar systems (Steiner, 1997). It is remarkable that for both positions of the disordered (*R*)-(1), the shortest contacts observed are between the O atoms that define the chirality, *i.e.* O1 and O7 and a hydrogen atom (H83 and H86) of the methoxy group of G3 and G6, the residues that tilt the least and move toward the guest. Fig. 8 shows two side views of the complex rotated by 90° around the TMαCD axis. In Fig. 8(*b*) it is clearly seen that the cavity flattens in the direction parallel to the flat surface of the penetrating acetal ring, as the least tilting glucose units, G3 and G6, approach the guest in a parallel fashion. Concomitantly, the H atoms of the methoxy group MeO3 make the closest contacts with the acetalic O atoms. The other view (Fig. 8*a*), shows that the secondary side of the cavity widens in the direction where the penetrating guest ring has the maximum width, as the remaining four residues tilt strongly away from the guest closing the macrocycle's primary side.

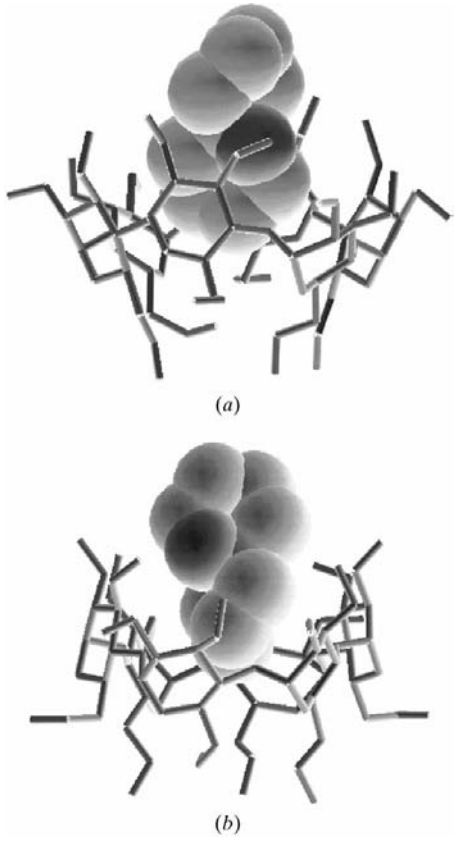

Figure 8
Two views of the TMαCD/(*R*)-(1) inclusion complex related by a 90° rotation about the molecular axis.

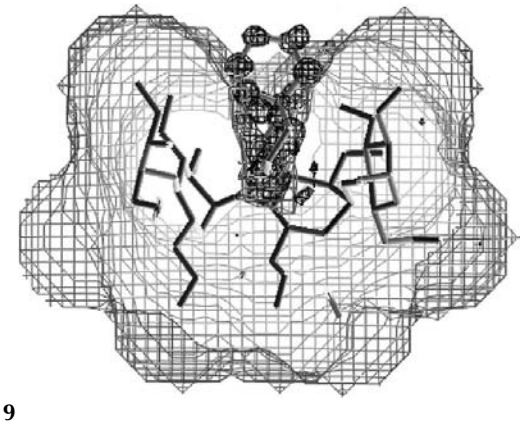

Figure 9
TMαCD/(*R*)-(1) inclusion complex. Calculated van der Waals surface of host (the front has been removed for clarity) and experimental difference electron density corresponding to the guest molecules, depicted as in Fig. 8(*a*).

Finally, the strong association of the host with the guest is reflected in the atomic thermal parameters of the latter. Usually, in cyclodextrin inclusion complexes the thermal parameters of the guest are an order of magnitude higher than those of the host, while in the present LT structure they are comparable, as they had also been in the RT structure, a fact indicating that the guest is strongly bound.

The above structural details are clearly reflected by our previously reported (Yannakopoulou *et al.*, 1996) measurements of binding constants in aqueous solution, which were 6800 M^{-1} for TMαCD/(*R*)-(1) and 4000 M^{-1} for TMαCD/(*S*)-enriched-(1). Both values are much higher than the presently measured binding constants of the corresponding complexes with TMβCD.

4. Conclusions

The crystal structure at 100 K of TMβCD/(*S*)-(1), determined for the first time, proved that TMβCD selectively crystallizes only the (*S*)-enantiomer from the racemic mixture. The high-resolution, low-temperature structures of TMβCD/(*S*)-(1) and TMαCD/(*R*)-(1) demonstrate clearly that weak but numerous host–guest interactions are responsible for the observed enantioselectivity and the stability of the inclusion complexes. The binding is achieved by a combination of the irregular tilting of the glucose units as well as the conformation of the methoxy groups leading to an induced fit of the host to complement the geometry of the guest. The phenomenon of induced fit is observed in per-derivatized CDs, but not in the natural macrocycles. The difference in the ability of the hosts to selectively bind one of the optical antipodes is reflected in very subtle differences in the H$\cdots$O intermolecular distances observed between host and guest. In TMβCD/(*S*)-(1), many weak C—H$\cdots$O interactions render it a sufficiently stable inclusion complex judging from its binding constant in aqueous solution ($\sim$935 M^{-1}) as opposed to that of TMβCD/(*R*)-(1) ($\sim$370 M^{-1}). However, in TMαCD/(*R*)-(1) two such interactions, directed toward the acetalic O atoms, which define the chirality of the guest, are stronger and lead to H$\cdots$O distances much shorter than the other H$\cdots$O distances in this complex and in TMβCD/(*S*)-(1). The increased stability in solution of TMαCD/(*R*)-(1) (K = 6800 M^{-1}) reveals the importance of the above short distances. Moreover, in TMαCD/(*R*)-(1) the C—H$\cdots$O contacts of the (*R*)-(1) enantiomer with other host molecules in the lattice may explain the coherence of the crystal and the high-yield precipitation of that complex from racemic (1) by driving the equilibrium in solution towards (*R*)-(1).

Induced fit should not be attributed only to the stabilization of host–guest interactions, but also to the stabilization of the host itself. In both complexes the guest is held at the secondary side of the CD cavity, leaving the primary side empty. The excessive tilting of certain glucose residues and the rotation of the primary methoxy groups toward the interior of the cavity is taking place in order to stabilize the macrocycles's geometry through C—H$\cdots$O hydrogen bonding of the primary methoxy groups. The same phenomenon is also observed in related cases where either the whole cavity (Steiner & Saenger, 1996) or part of it is empty (Rontoyianni *et al.*, 1998; Caira *et al.*, 1994).

The present diffraction experiments have shown that synchrotron radiation of very short wavelength, combined with low temperatures, give accurate high-resolution data that reveal H-atom positions even for the guest and solvent molecules, something that before was possible only with neutron diffraction data. Although the crystals of cyclodextrin inclusion complexes are not perfect, it was possible to describe the exact host–guest interactions that lead to the observed macroscopic characteristics or reactivity of the system. Furthermore, it was also possible to describe fine details such as the disorder of labile groups or solvent molecules, where stabilization through weak intermolecular interactions can occur in more than one way. Finally, the detailed hydrogen bonding and geometry of the five-membered ring water cluster in TMαCD(1) provides valuable experimental evidence towards understanding interactions between water molecules. Thus, cyclodextrins that are used as artificial enzymes performing biomimetic chemistry and share some of the characteristics and drawbacks of macromolecular systems, such as cocrystallization with water molecules and disorder, can teach us about intermolecular interactions in larger and more complicated systems.

We would like to thank European Program VALUE CTT 472 for funding, and Drs F. Krokos and V. Mazomenos for use of their chiral GC facility. We also thank the European Union for support of the work at EMBL outstation, DESY, Hamburg through the HCMP Access to Large Installations Project, Contract Number CHGE-CT93-0040.

References

Benshop, H. P. & Van der Berg, G. R. (1970). *J. Chem. Soc. Chem. Commun.* pp. 1435–1436.
Beurskens, P. T., Admiraal, G., Beurskens, G., Bosman, W. P., de Gelder, R., Israel, R. & Smits, J. M. M. (1994). *The DIRDIF94 Program System.* Crystallography Laboratory, University of Nijmegen, The Netherlands.
Breslow, R. & Dong, S. D. (1998). *Chem. Rev.* **98**, 1997–2011.
Brown, G. R., Caira, M. R., Nassimbeni, L. R. & VanOudtshoon, B. (1996). *J. Incl. Phenom.* **26**, 281–294.
Caira, M. R., Griffith, V. J., Nassimbeni, L. R. & VanOudtshoon, B. (1994). *J. Chem. Soc. Perkin Trans. 2*, pp. 2071–2072.
Caira, M. R., Griffith, V. J., Nassimbeni, L. R. & VanOudtshoon, B. (1995). *J. Incl. Phenom.* **20**, 277–290.
Caira, M. R., Griffith, V. J., Nassimbeni, L. R. & VanOudtshoon, B. (1996). *Supramol. Chem.* **7**, 119–124.
Egert, E. & Sheldrick, G. M. (1985). *Acta Cryst.* A**41**, 262–268.
Fletcher, M. T. & Kitching, W. (1995). *Chem. Rev.* **95**, 789–828.
Hamilton, J. A. & Chen, L. (1988). *J. Am. Chem. Soc.* **110**, 5833–5841.
Harata, K. (1990). *J. Chem. Soc. Perkin Trans. 2*, pp. 799–804.
Harata, K., Hirayama, F., Arrima, H., Uekama, K. & Miyaji, T. (1992). *J. Chem. Soc. Perkin Trans. 2*, pp. 1159–1166.
Harata, K., Uekama, K., Imai, T., Hirayama, F. & Otagiri, M. (1988). *J. Incl. Phenom.* **6**, 443–460.
Harata, K., Uekama, K. & Otagiri, M. (1987). *Bull. Chem. Soc. Jpn*, **60**, 497–502.
Harata, K., Uekama, K., Otagiri, M. & Hirayama, F. (1982*a*). *Bull. Chem. Soc. Jpn*, **55**, 407–410.

Harata, K., Uekama, K., Otagiri, M. & Hirayama, F. (1982*b*). *Bull. Chem. Soc. Jpn*, **55**, 3904–3910.
Harata, K., Uekama, K., Otagiri, M. & Hirayama, F. (1983). *Bull. Chem. Soc. Jpn*, **56**, 1732–1736.
Harata, K., Uekama, K., Otagiri, M. & Hirayama, F. J. (1984*a*). *J. Incl. Phenom.* **1**, 279–293.
Harata, K., Uekama, K., Otagiri, M. & Hirayama, F. (1984*b*). *J. Incl. Phenom.* **2**, 583–594.
Harata, K., Uekama, K., Otagiri, M., Hirayama, F. & Sugiyama, Y. (1982). *Bull. Chem. Soc. Jpn*, **55**, 3386–3389.
Hilton, M. L. & Armstrong, D. W. (1991). *New Trends in Cyclodextrins and Derivatives*, edited by D. Duchêne, pp. 515–549. Paris, France: Editions de Santé.
Köhler, J. E. H., Hohla, M., Richters, M. & König, W. A. (1992). *Angew. Chem. Int. Ed. Engl.* **31**, 319–320.
König, W. A. (1991). *New Trends in Cyclodextrins and Derivatives*, edited by D. Duchêne, pp. 551–594. Paris, France: Editions de Santé.
Lehn, J.-M. (1995). *Supramolecular Chemistry*, pp. 11–30. Weinheim: VCH.
Li, S. & Purdy, W. C. (1992). *Chem. Rev.* **92**, 1457–1470.
Mentzafos, D., Mavridis, I. M., Le Bas, G. & Tsoucaris, G. (1991). *Acta Cryst.* B**47**, 746–757.
Mentzafos, D., Mavridis, I. M. & Schenk, H. (1994). *Carbohydr. Res.* **253**, 39–50.
Mentzafos, D., Mavridis, I. M. & Yannakopoulou, K. (1999). *J. Incl. Phenom.* **33**, 321–330.
Mokolajczyk, M. & Drabowicz, J. (1971). *J. Chem Soc. Chem. Commun.* pp. 317–318.
Mori, K. (1998). *Eur. J. Org. Chem.* pp. 1479–1489.
Otwinowski, Z. & Minor, W. (1997). *Processing of X-ray Diffraction Data Collected in Oscillation Mode, Methods in Enzymology*, p. 276: *Macromolecular Crystallography*, Part A, edited by C. W. Carter Jr and R. M. Sweet, pp. 307–326. New York: Academic Press.
Rontoyianni, A., Mavridis, I. M., Israel, R. & Beurskens, G. (1998). *J. Incl. Phenom.* **32**, 415–428.
Rysanek, N., Le Bas, G., Villain, F. & Tsoucaris, G. (1992). *Acta Cryst.* C**48**, 1466–1471.
Saenger, W. (1980). *Angew. Chem. Int. Ed. Engl.* **19**, 344–362.
Schürig, V. & Nowotny, H.-P. (1990). *Angew. Chem. Int. Ed. Engl.* **29**, 939–956.
Sheldrick, G. M. (1997). *SHELX*97. University of Göttingen, Germany.
Steiner, T. (1997). *J. Chem. Soc. Chem. Commun.* pp. 727–734.
Steiner, T. & Desiraju, G. R. (1998). *J. Chem. Soc. Chem. Commun.* pp. 891–892.
Steiner, T. & Saenger, W. (1996). *Carbohydr. Res.* **282**, 53–63.
Szejtli, J. (1998). *Chem. Rev.* **98**, 1743–1753.
Wenz, G. (1994). *Angew. Chem. Int. Ed. Engl.* **33**, 803–822.
Yannakopoulou, K., Mentzafos, D., Mavridis, I. M. & Dandika, K. (1996). *Angew. Chem. Int. Ed. Engl.* **35**, 2480–2482.
Zabel, V., Saenger, W. & Mason, S. A. (1986). *J. Am. Chem. Soc.* **108**, 3664–3673.